

Rashba effect and enriched spin-valley coupling in GaX/MX_2 ($M = \text{Mo}, \text{W}; X = \text{S}, \text{Se}, \text{Te}$) heterostructures

Qingyun Zhang and Udo Schwingenschlöggl*

Physical Science and Engineering Division, King Abdullah University of Science and Technology, Thuwal 23955-6900, Saudi Arabia

(Received 3 November 2017; revised manuscript received 21 January 2018; published 16 April 2018)

Using first-principles calculations, we investigate the electronic properties of the two-dimensional GaX/MX_2 ($M = \text{Mo}, \text{W}; X = \text{S}, \text{Se}, \text{Te}$) heterostructures. Orbital hybridization between GaX and MX_2 is found to result in Rashba splitting at the valence-band edge around the Γ point, which grows for increasing strength of the spin-orbit coupling in the p orbitals of the chalcogenide atoms. The location of the valence-band maximum in the Brillouin zone can be tuned by strain and application of an out-of-plane electric field. The coexistence of Rashba splitting (in-plane spin direction) and band splitting at the K and K' valleys (out-of-plane spin direction) makes GaX/MX_2 heterostructures interesting for spintronics and valleytronics. They are promising candidates for two-dimensional spin-field-effect transistors and spin-valley Hall effect devices. Our findings shed light on the spin-valley coupling in van der Waals heterostructures.

DOI: [10.1103/PhysRevB.97.155415](https://doi.org/10.1103/PhysRevB.97.155415)

I. INTRODUCTION

Monolayers of transition-metal dichalcogenides (such as MoS_2 , MoTe_2 , and WSe_2) nowadays are receiving immense interest for both fundamental and applied reasons [1–4]. They can be fabricated by mechanical exfoliation due to weak layer-layer interaction in the respective bulk compounds [5,6]. The H phase shows band splitting at the K and K' valleys since there is no inversion symmetry [7,8], which is key for the field of valleytronics [9,10], i.e., the manipulation and utilization of the valley degree of freedom. Valley polarization by circularly polarized light was first proposed theoretically and subsequently was realized by several experimental groups [11,12]. Van der Waals heterostructures based on transition-metal dichalcogenides and other two-dimensional materials, such as graphene, h -BN, and black phosphorus, currently are starting to attract a lot of interest in both experiment and theory [13–16]. Novel electronic and optical properties have been discovered, for example, interlayer excitons (due to the type-II band alignment between MoS_2 and WS_2) that have a much longer lifetime than intralayer excitons [17]. In graphene/ MoS_2 heterostructures small band gaps are observed above the Dirac point that result from perturbation by the interlayer interaction [18]. Although the van der Waals interaction is much weaker than ionic and covalent bonds, it can still alter the electronic properties of a material. Examples are the band gap opening from monolayer to bilayer graphene [19] and the direct to indirect band gap transition from monolayer to bilayer transition-metal dichalcogenides [6].

In heterostructures and at surfaces the Rashba effect can play a decisive role for the electronic states because the structural asymmetry causes an out-of-plane electric field. For a two-dimensional electron gas the Rashba effect is described by the Hamiltonian $H_R = \alpha_R \hat{\sigma} \cdot (\hat{k}_{\parallel} \times \hat{e}_z)$, where α_R is the

Rashba parameter, $\hat{\sigma}$ is the vector of the Pauli matrices, $\hat{k}_{\parallel} = (k_x, k_y, 0)$ is the in-plane momentum of the electrons, and \hat{e}_z is the out-of-plane unit vector [20]. The Rashba effect has been studied intensively in the realm of spintronics since it can be used to tune the spin direction by means of an electric field. Experimentally, it has been observed in semiconductor quantum wells [21,22], surfaces of heavy metals [23–26], and polar semiconductors like BiTeI [27]. Theoretical insights have been reported for several two-dimensional materials, in particular graphene [28,29], LaOBiS_2 films [30], polar transition-metal dichalcogenide monolayers [31], and the $\text{MoS}_2/\text{Bi}(111)$ heterostructure [32].

Two-dimensional Ga chalcogenides have a hexagonal structure and are indirect band gap semiconductors [33]. A very recent experimental study of the $\text{GaSe}/\text{MoSe}_2$ heterostructure found that the interaction between the components is strong [34], while theoretical insights are missing so far. In the present work we therefore investigate the electronic properties of the GaX/MX_2 ($M = \text{Mo}, \text{W}; X = \text{S}, \text{Se}, \text{Te}$) heterostructures and demonstrate Rashba splitting at the valence band edge around the Γ point. Tuning the band edges by strain and an out-of-plane external electric field is addressed. Due to the semiconductor nature of the heterostructures, combining Rashba splitting with the well-known band splitting at the K and K' valleys is interesting for both spintronics and valleytronics applications.

II. COMPUTATIONAL DETAILS

Methodologically, we conduct structure relaxations and subsequent band structure calculations using the Vienna Ab initio Simulation Package (VASP) [35]. The generalized gradient approximation as parametrized by Perdew, Burke, and Ernzerhof (PBE) [36] is employed with the kinetic-energy cutoff set to 400 eV. For the Brillouin zone sampling a $6 \times 6 \times 1$ k mesh is used. Spin-orbit coupling is not included during the structure relaxations but is added in the band structure calculations. A vacuum thickness of 17 Å is adopted

*Udo.Schwingenschlöggl@kaust.edu.sa

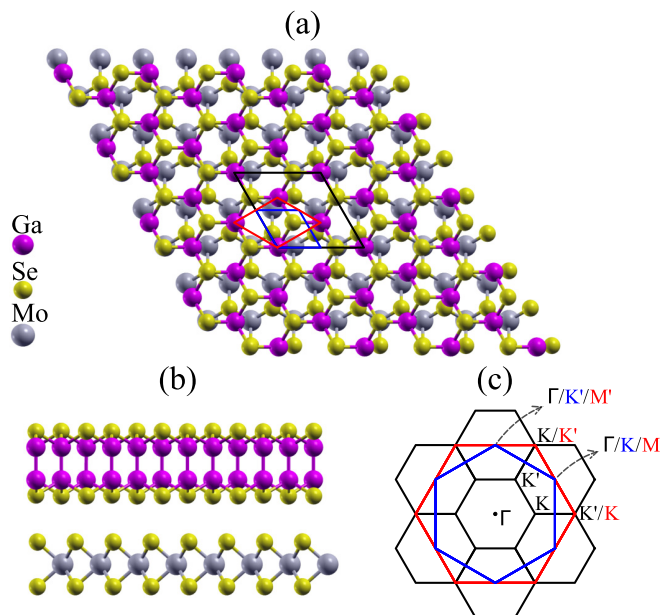


FIG. 1. (a) Side and (b) top views of the GaSe/MoSe₂ heterostructure, which is also representative of the other heterostructures under study. (c) Brillouin zones of the heterostructure (black), pristine monolayer GaSe (blue), and pristine monolayer MoSe₂ (red).

to avoid interaction between the top and bottom surfaces in the slab model. Due to different lattice constants, heterostructures are built from $\sqrt{3} \times \sqrt{3} \times 1$ supercells of GaX and $2 \times 2 \times 1$ supercells of MX_2 . Three approaches to model the van der Waals interaction (DFT-D3 [37], optB88-vdW [38], and optB86b-vdW [39]) are adopted in the structure relaxations, which are continued until the forces on all atoms have declined to less than 0.005 eV/Å. It turns out that an increase in the energy cutoff to 500 eV modifies the total energy by less than 1 meV for each heterostructure. In addition, application of a finer $8 \times 8 \times 1$ k mesh modifies the total energy by less than 5 meV per GaX or MX_2 unit cell. Both GaX and MX_2 have D_{3h} symmetry (threefold in-plane rotation symmetry and out-of-plane mirror symmetry), while the structural relaxation in the heterostructure slightly breaks the rotation symmetry.

The lowest-energy configuration of the GaSe/MoSe₂ heterostructure is shown in Fig. 1 as an example. Lateral shifts between the components are found to modify the total energy

by less than 10 meV and have minor effects on the band structure and spin texture. The relaxed GaSe/MoSe₂ heterostructure is adopted as the starting point for building the other heterostructures. Relaxed lattice constants, interlayer distances, and binding energies per unit cell of MX_2 are summarized in Table I. We find that the DFT-D3 and optB86b-vdW methods lead to very similar results for the lattice constants and interlayer distances, while the optB88-vdW method yields larger lattice constants and slightly larger interlayer distances. The binding energies obtained for the three methods are close to each other. The DFT-D3 method gives the smallest lattice constants for the GaS/MoS₂ and GaS/WS₂ heterostructures and the largest for the other heterostructures. Since the experimental lattice constant of monolayer MoSe₂ is 3.29 Å, which clearly deviates from the result of the optB88-vdW method, we adopt the DFT-D3 method in the following.

III. RESULTS AND DISCUSSION

The GaSe/MoSe₂ heterostructure is taken as a representative example to study the electronic properties using the PBE functional. Pristine monolayer GaSe is reported to have a lattice constant of 3.82 Å and to be an indirect band gap (1.75 eV) semiconductor with the conduction-band minimum located at the Γ point and the valence band resembling a Mexican hat [33]. Pristine monolayer MoSe₂ is a direct band gap (1.33 eV; at the K point) semiconductor with a lattice constant of 3.32 Å [7]. The band structure of GaSe/MoSe₂ obtained by our calculations without spin-orbit coupling is shown in Fig. 2(a), exhibiting an indirect band gap of 1.46 eV. The conduction-band minimum is located at the Γ point, and the valence-band maximum is located at the K point. Orbital projections show that the valence- and conduction-band edges are due to MoSe₂ and GaSe, respectively. However, there is strong hybridization between the component monolayers in the highest valence band around the Γ point, which is confirmed by the density of states in Fig. 2(b). A similar hybridization is also found in MoX₂/WX₂ heterostructures [40]. When the spin-orbit coupling is turned on [see Fig. 2(c)], band splitting is observed due to inversion symmetry breaking, except for the time-reversal-invariant k points. Strong splitting of the highest valence band at the K point is expected since it traces back to MoSe₂. The band splitting observed at the Γ point, however, is not found in the component monolayers, which means that it is due to the interaction in the heterostructure. It reveals close

TABLE I. Lattice constants a_0 , interlayer distances d_i , and binding energies E_b obtained for different functionals. The lattice mismatch δ of the monolayers is also given.

	DFT-D3			optB86b-vdW			optB88-vdW			δ (%)
	a_0 (Å)	d_i (Å)	E_b (meV)	a_0 (Å)	d_i (Å)	E_b (meV)	a_0 (Å)	d_i (Å)	E_b (meV)	
GaS/MoS ₂	6.309	3.355	156	6.305	3.335	163	6.354	3.357	167	1.0
GaSe/MoSe ₂	6.582	3.463	179	6.579	3.456	173	6.633	3.484	176	0.2
GaTe/MoTe ₂	7.076	3.820	195	7.070	3.767	190	7.134	3.821	190	0.9
GaS/WS ₂	6.312	3.348	159	6.305	3.331	163	6.352	3.364	166	1.0
GaSe/WSe ₂	6.576	3.445	185	6.577	3.424	172	6.629	3.500	175	0.1
GaTe/WTe ₂	7.070	3.780	201	7.069	3.740	190	7.136	3.807	190	0.8

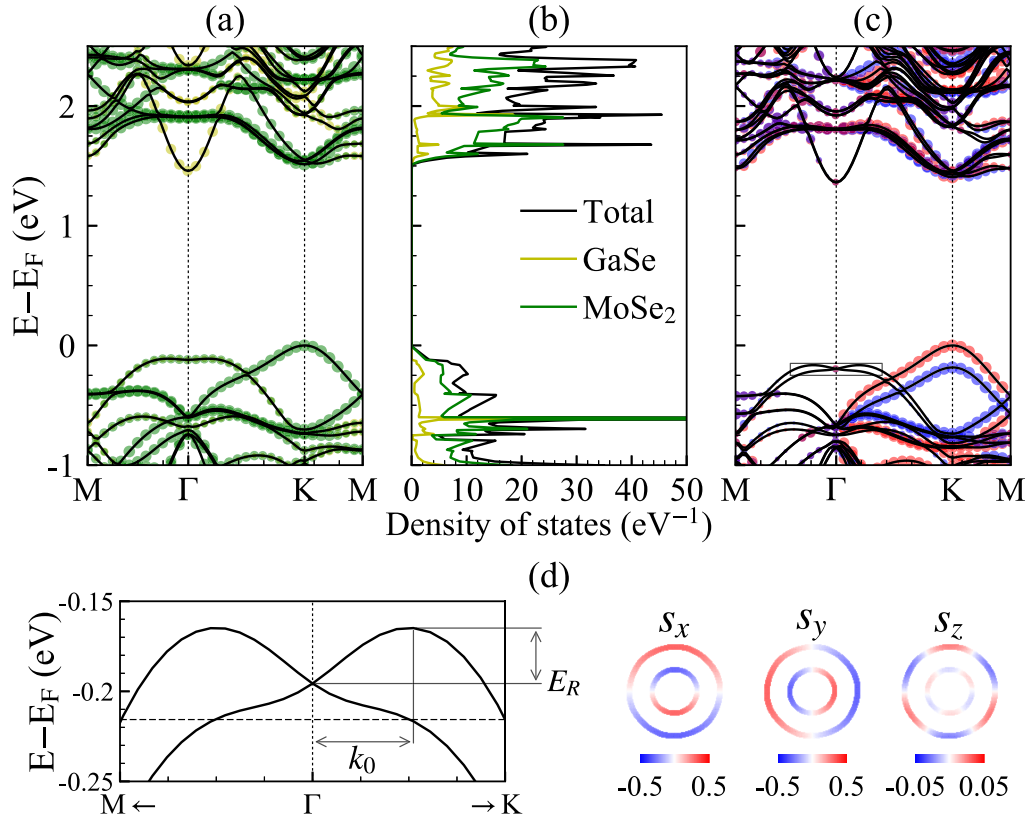


FIG. 2. (a) Band structure of the GaSe/MoSe₂ heterostructure obtained without spin-orbit coupling. The size of the circles denotes the projection on GaSe (yellow) and MoSe₂ (green). (b) Corresponding density of states. (c) Band structure obtained with spin-orbit coupling. The size of the circles denotes the spin projection in the out-of-plane direction, and red and blue indicate positive and negative values, respectively. (d) Zoom of the marked region and spin components in constant-energy cuts at the dashed line.

similarity to the Rashba splitting in semiconductor quantum wells and surfaces of heavy metals [21–26]. In the following, we first study the valence-band edge around the Γ point (while the valence-band maximum appears at the K point) and later deal with approaches to tune the energies of the band edges at the Γ and K points relative to each other.

We address the spin components close to the Γ point in Fig. 2(d). While the spin direction is mainly in plane, the constant-energy cuts show outer and inner circles with clockwise and counterclockwise rotating spin directions, respectively. This pattern is consistent with the characteristics of the Rashba Hamiltonian [20]. The origin of the small out-of-plane spin component is the in-plane electric field due to the absence of inversion symmetry. For a two-dimensional system with C_{3v} symmetry, we can apply the effective Hamiltonian [27]

$$H(k) = \hbar^2 k^2 / 2m^* + \alpha_R (k_x \sigma_y - k_y \sigma_x) + \lambda k^3 \sin(3\theta) \sigma_z, \quad (1)$$

where $k = \sqrt{k_x^2 + k_y^2}$, m^* is the effective mass, θ is the azimuthal angle of momentum, and λ is the warping parameter. The second and third terms of $H(k)$, respectively, will cause in-plane and out-of-plane spin polarization, so that the spin polarization at fixed energy is given by $P(\theta) \sim [\pm \alpha_R \sin\theta, \mp \alpha_R \cos\theta, \mp \lambda k^2 \sin(3\theta)]$, in agreement with the spin component plots in Fig. 2(d). The strength of the Rashba splitting can be characterized by the momentum offset k_0 and energy difference E_R between the valence-band maximum and the band crossing

at the Γ point [see Fig. 2(d)]. These quantities are related to the Rashba parameter α_R by $E_R = \hbar^2 k_0^2 / 2m^*$ and $k_0 = m^* \alpha_R / \hbar^2$. Although the band structures turn out to be not exactly parabolic as in the case of the Rashba Hamiltonian for a two-dimensional electron gas, the relation $\alpha_R = 2E_R / k_0$ still gives a good estimation of the Rashba parameter. For the GaSe/MoSe₂ heterostructure we obtain $E_R = 31$ meV and $k_0 = 0.13 \text{ \AA}^{-1}$, so that $\alpha_R = 0.49 \text{ eV \AA}$. A comparison of selected materials is given in Table II. The magnitude of Rashba splitting obtained for the GaSe/MoSe₂ heterostructure is comparable to that of Au(111) and Bi(111) surfaces [23,24] and much larger than reported for the InGaAs/InAlAs quantum well [21]. We notice that the conduction-band edge at the

TABLE II. Parameters characterizing the Rashba splitting in selected materials.

	E_R (meV)	k_0 (\AA^{-1})	α_R (eV \AA)
InGaAs/InAlAs quantum well [21]	< 1	0.028	0.07
Au(111) surface [23]	2.1	0.012	0.33
Bi(111) surface [24]	14	0.05	0.55
Bi/Ag(111) surface alloy [25]	200	0.13	3.05
BiTeI [27]	100	0.052	3.8
GaSe/MoSe ₂ heterostructure (this work)	31	0.13	0.49

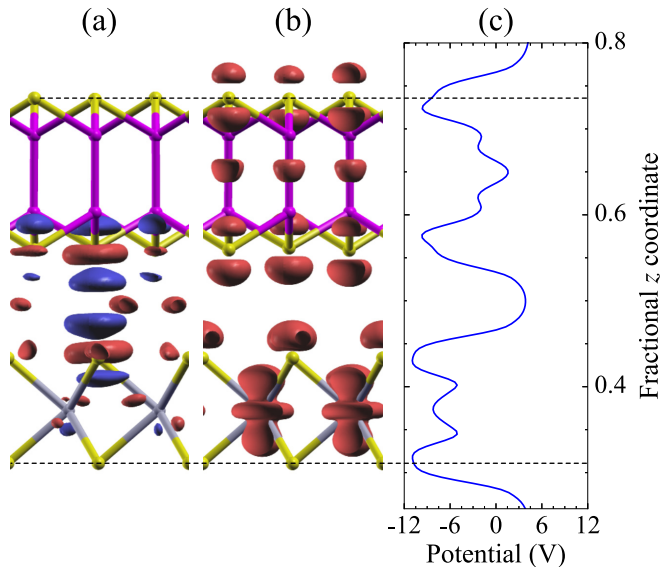


FIG. 3. (a) Charge-density difference due to the interfacial interaction (isosurface value: $0.001 \text{ electron}/\text{\AA}^3$). (b) Charge density in the highest valence band at the Γ point (isosurface value: $0.015 \text{ electron}/\text{\AA}^3$). (c) Plane-averaged electrostatic potential along the out-of-plane direction. The dashed lines highlight the positions of the top and bottom atoms.

Γ point also exhibits a slight band splitting, with the spin directions resembling those at the valence-band edge.

The Rashba effect in a two-dimensional electron gas requires an out-of-plane electric field. In our case Rashba splitting is achieved by interaction between GaX and MX_2 , as the degeneracy of the inner and outer chalcogenide atoms is lifted. We plot the charge-density difference between the GaSe/MoSe₂ heterostructure and its noninteracting components in Fig. 3(a), showing charge redistribution around the interface. To highlight the hybridization between the component monolayers, we depict the charge density in the highest valence band at the Γ point in Fig. 3(b). Most contributions are due to the Se p orbitals (of both GaSe and MoSe₂) and the Mo d orbitals, with small admixtures of the Ga s, p orbitals. Figure 3(b) therefore illustrates the lifted degeneracy of the inner and outer chalcogenide atoms that results in Rashba splitting. It may be speculated that encapsulation of the heterostructure, for example, by hexagonal boron nitride, would reduce the difference in the electrostatic potential between the inner and outer chalcogenide atoms and, consequently, would tend to attenuate the Rashba splitting. The plane-averaged electrostatic potential (with dipole correction) shown in Fig. 3(c) demonstrates that the charge redistribution results in a small potential step between the component monolayers.

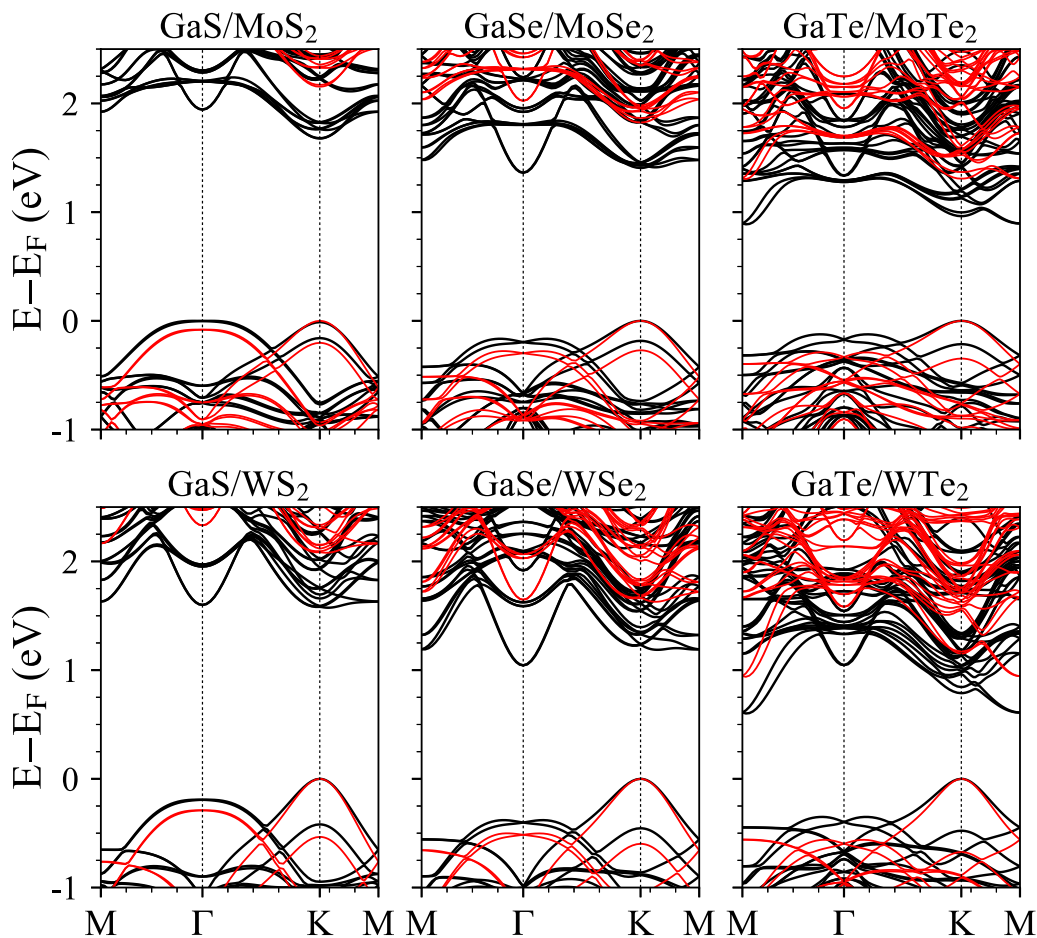


FIG. 4. Band structures of the GX/MX_2 ($M = \text{Mo, W}; X = \text{S, Se, Te}$) heterostructures. Black and red lines represent results of PBE and HSE06 calculations, respectively.

TABLE III. Rashba parameters and band splittings at the K valleys ΔE_K .

	PBE			HSE06		
	E_R (meV)	k_0 (\AA^{-1})	ΔE_K (meV)	E_R (meV)	k_0 (\AA^{-1})	ΔE_K (meV)
GaS/MoS ₂	2	0.05	147	1	0.04	202
GaSe/MoSe ₂	31	0.13	184	20	0.11	271
GaTe/MoTe ₂	48	0.12	215	43	0.12	347
GaS/WS ₂	1	0.03	419	1	0.03	533
GaSe/WSe ₂	22	0.11	455	14	0.09	598
GaTe/WTe ₂	47	0.11	477	37	0.10	674

The PBE band structures of the six heterostructures under investigation are shown in Fig. 4 (black lines). We notice systematic differences which are due to different band offsets between GaX and MX_2 as well as the residual strain resulting from the small but finite lattice mismatches. It is known that in monolayer MX_2 the relative position of the valence-band edges at the Γ and K points is sensitive to strain [41–44]. In Fig. 4 the band splittings at both the Γ and K points are enhanced from top to bottom (due to the increasing strength of the spin-orbit coupling in the p orbitals of the chalcogenide atoms), and the band gaps shrink. We also present in Fig. 4 (red lines) results of Heyd-Scuseria-Ernzerhof (HSE06) calculations in order to improve the prediction of band gap sizes. In each case the HSE06 functional results in an enlarged band gap compared to the PBE functional since the valence-band edge (Γ point) shifts to lower energy. In addition, the band splitting at the K point is enhanced, in agreement with previous studies [45,46]. The Rashba coefficients obtained from the six band structures in Fig. 4 are summarized in Table III.

It is an interesting observation that, despite large contributions from the transition-metal d orbitals, the Rashba splitting decreases when Mo is replaced with W (which is opposite to the trend of the band splitting at the K point). On the other hand, at the valence-band edge around the Γ point this replacement enhances d -orbital contributions at the expense of p -orbital contributions. Therefore, not the d but the p orbitals are responsible for the Rashba splitting, similar to observations for the MoS₂/Bi(111) system [32]. The fact that the Rashba splitting in the GaS/MS₂ heterostructure is much smaller than in the GaSe/MSe₂ and GaTe/MTe₂ heterostructures can result from two reasons: first, that the spin-orbit coupling is weaker for S than for Se/Te and, second, that the p -orbital contributions of the outer chalcogenide atoms at the valence-band edge around the Γ point are enhanced (as this lowers the difference with respect to the inner chalcogenide atoms). As expected, the HSE06 functional lowers the value of E_R for all heterostructures due to reduced p -orbital contributions.

The band structure of the GaSe/MoSe₂ heterostructure in Fig. 5(a) shows for 2% tensile strain that the valence-band edge around the Γ point shifts to higher energy and approaches that at the K point. The fact that the band gap decreases is expected since the band gaps of both GaSe and MoSe₂ are suppressed by strain [47]. The variation of the energetic difference between

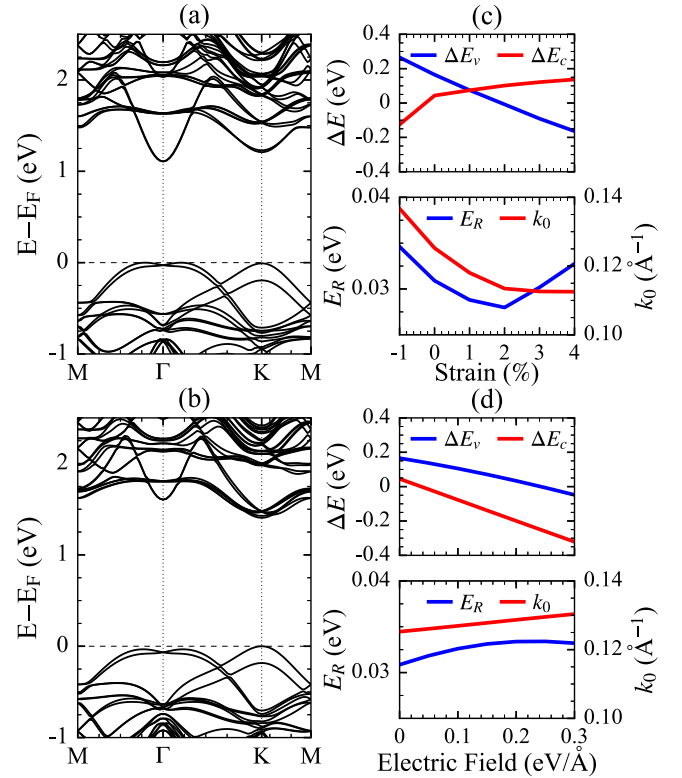


FIG. 5. GaSe/MoSe₂ heterostructure (a) and (c) under 2% biaxial tensile strain and (b) and (d) in a 0.2 V/Å out-of-plane electric field: band structures and corresponding variations of the band edges and Rashba parameters.

the two valence-/conduction-band edges under strain,

$$\Delta E_{v/c} = E_{v/c}(K) - E_{v/c}(\Gamma), \quad (2)$$

is addressed in the top panel of Fig. 5(c). We observe an almost linear behavior of ΔE_v . The valence-band maximum shifts off the K point at about 2% tensile strain, and the conduction-band minimum shifts from the Γ to the K point at small compressive strain. According to the bottom panel in Fig. 5(c), E_R shows a minimum around 2% tensile strain, while k_0 decreases up to 4% tensile strain. Because an external out-of-plane electric field is also an effective method to tune the electronic properties, the band structure of the GaSe/MoSe₂ heterostructure in an electric field of 0.2 eV/Å is given in Fig. 5(b). The valence-band edge around the Γ point is found to be shifted to higher energy. On the other hand, the band gap is subject to only minor changes since the electric field affects the valence and conduction bands in a similar way [see the bottom panel in Fig. 5(d)], both exhibiting an almost linear behavior. The valence band is less affected due to the mentioned hybridization around the Γ point. It turns out that E_R and k_0 are slightly enhanced. As strain and an external electric field modify the energetic positions of the valence-band edges, for both these approaches a small hole doping can be used to tune the carrier populations in the different pockets of the Brillouin zone. Since the pockets correspond to different spin directions, this fact gives rise to a new methodology for spin manipulation in spintronics applications.

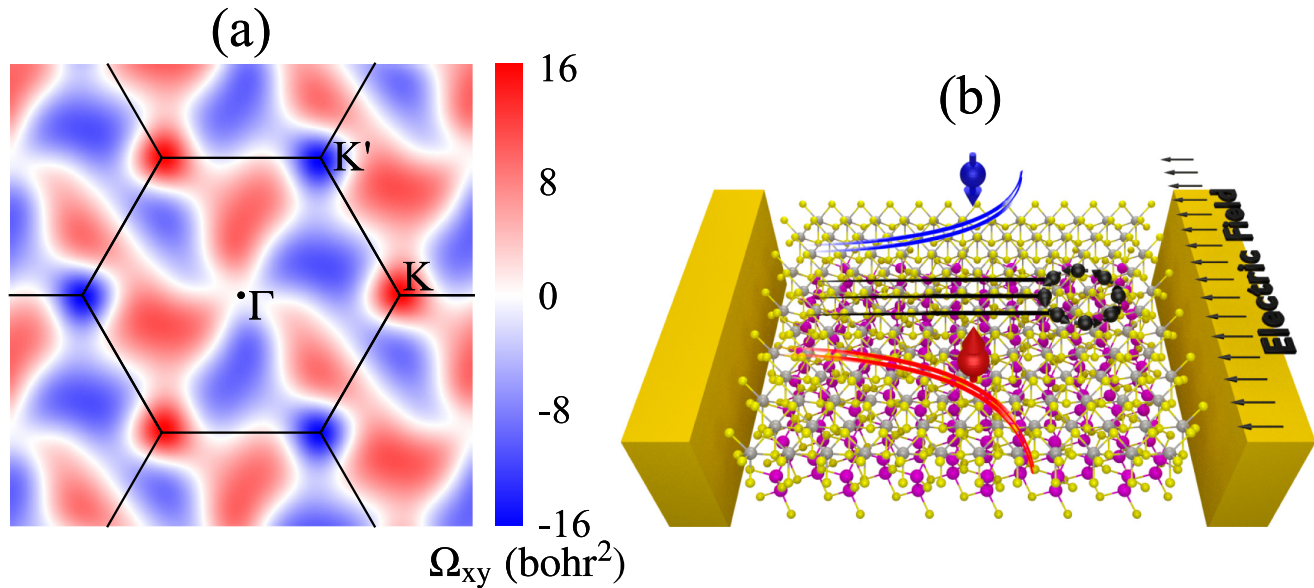


FIG. 6. (a) Berry curvature and (b) schematic illustration of the electron transport in an in-plane electric field.

In monolayer transition-metal dichalcogenides the spin and valley degrees of freedom are coupled because of the spin-orbit coupling and inversion symmetry breaking. The Berry curvature has opposite values at the K and K' points, which leads to spin and valley Hall effects [8]. Since the valley properties remain the same in the heterostructures under consideration, we derive the Berry curvature by means of the Wannier interpolation method of the WANNIER90 code [48] [see the results in Fig. 6(a)]. We obtain maximal values with opposite sign at the K and K' points, similar to pristine MX_2 [49]. That the Berry curvature is smaller around the Γ point implies that the spin-up electrons at the K valley, the spin-down electrons at the K' valley, and the in-plane spin electrons around the Γ point follow three different transport paths in the presence of an in-plane electric field. Figure 6(b) gives a schematic picture of these three paths. The coexistence of Rashba splitting (in-plane spin direction) and band splitting at the K and K' valleys (out-of-plane spin direction) is interesting for both spintronics and valleytronics.

IV. CONCLUSION

In conclusion, our first-principles results on the electronic properties of the GaX/MX_2 ($M = Mo, W$; $X = S, Se, Te$) heterostructures demonstrate hybridization between the states of the component monolayers around the Γ point, which leads to Rashba splitting. Since the Berry curvature has different values at the K , K' , and Γ points, three different transport paths apply to electrons with out-of-plane (up and down) and

in-plane spin polarizations. Both strain and an out-of-plane electric field can be employed to tune the location of the valence-band maximum in the Brillouin zone, providing new schemes to manipulate the spin direction of doped holes. While the coexistence of Rashba splitting and band splitting at the K and K' valleys has been demonstrated before in the metallic $MoS_2/Bi(111)$ heterostructure, the semiconducting nature of the experimentally available $GaSe/MoSe_2$ heterostructure paves the way to new device applications, as the spin direction can be manipulated effectively by an electric field. For example, spin accumulation resulting from spin-momentum locking [50–52] or the spin Hall effect [53–55] will exert spin-transfer torque on an adjacent magnet. In order to control the direction of this spin-transfer torque, it is necessary to control the spin direction in the heterostructure. From the perspective of the component materials, it is critical that monolayer MX_2 provides the band splitting with the out-of-plane spin direction together with similar energies of the valence-band edges at the Γ and K points. Our results leave no doubt that GaX/MX_2 ($M = Mo, W$; $X = S, Se, Te$) heterostructures are highly promising candidates for realizing new concepts in spintronics and valleytronics.

ACKNOWLEDGMENT

The research reported in this publication was supported by funding from King Abdullah University of Science and Technology (KAUST).

- [1] B. Radisavljevic, A. Radenovic, J. Brivio, V. Giacometti, and A. Kis, Single-layer MoS_2 transistors, *Nat. Nanotechnol.* **6**, 147 (2011).
 [2] Q. H. Wang, K. Kalantar-Zadeh, A. Kis, J. N. Coleman, and M. S. Strano, Electronics and optoelectronics of two-dimensional transition metal dichalcogenides, *Nat. Nanotechnol.* **7**, 699 (2012).

- [3] A. Castellanos-Gomez, M. Poot, G. A. Steele, H. S. J. van der Zant, N. Agrait, and G. Rubio-Bollinger, Elastic properties of freely suspended MoS_2 nanosheets, *Adv. Mater.* **24**, 772 (2012).
 [4] H. Fang, S. Chuang, T. C. Chang, K. Takei, T. Takahashi, and A. Javey, High-performance single layered WSe_2 p -FETs with chemically doped contacts, *Nano Lett.* **12**, 3788 (2012).

- [5] A. Splendiani, L. Sun, Y. Zhang, T. Li, J. Kim, C.-Y. Chim, G. Galli, and F. Wang, Emerging photoluminescence in monolayer MoS₂, *Nano Lett.* **10**, 1271 (2010).
- [6] K. F. Mak, C. Lee, J. Hone, J. Shan, and T. F. Heinz, Atomically Thin MoS₂: A New Direct-Gap Semiconductor, *Phys. Rev. Lett.* **105**, 136805 (2010).
- [7] Z. Y. Zhu, Y. C. Cheng, and U. Schwingenschlöggl, Giant spin-orbit-induced spin splitting in two-dimensional transition-metal dichalcogenide semiconductors, *Phys. Rev. B* **84**, 153402 (2011).
- [8] D. Xiao, G.-B. Liu, W. X. Feng, X. D. Xu, and W. Yao, Coupled Spin and Valley Physics in Monolayers of MoS₂ and Other Group-VI Dichalcogenides, *Phys. Rev. Lett.* **108**, 196802 (2012).
- [9] A. Rycerz, J. Tworzydło, and C. W. J. Beenakker, Valley filter and valley valve in graphene, *Nat. Phys.* **3**, 172 (2007).
- [10] D. Xiao, W. Yao, and Q. Niu, Valley-Contrasting Physics in Graphene: Magnetic Moment and Topological Transport, *Phys. Rev. Lett.* **99**, 236809 (2007).
- [11] H. L. Zeng, J. F. Dai, W. Yao, D. Xiao, and X. D. Cui, Valley polarization in MoS₂ monolayers by optical pumping, *Nat. Nanotechnol.* **7**, 490 (2012).
- [12] T. Cao, G. Wang, W. Han, H. Ye, C. Zhu, J. Shi, Q. Niu, P. Tan, E. Wang, B. Liu, and J. Feng, Valley-selective circular dichroism of monolayer molybdenum disulphide, *Nat. Commun.* **3**, 887 (2012).
- [13] M.-Y. Li, C.-H. Chen, Y. Shi, and L.-J. Li, Heterostructures based on two-dimensional layered materials and their potential applications, *Mater. Today* **19**, 322 (2016).
- [14] G. R. Bhimanapati, Z. Lin, V. Meunier, Y. Jung, J. Cha, S. Das, D. Xiao, Y. Son, M. S. Strano, V. R. Cooper, L. Liang, S. G. Louie, E. Ringe, W. Zhou, S. S. Kim, R. R. Naik, B. G. Sumpter, H. Terrones, F. Xia, Y. Wang, J. Zhu, D. Akinwande, N. Alem, J. A. Schuller, R. E. Schaak, M. Terrones, and J. A. Robinson, Recent advances in two-dimensional materials beyond graphene, *ACS Nano* **9**, 11509 (2015).
- [15] K. S. Novoselov, A. Mishchenko, A. Carvalho, and A. H. Castro Neto, 2D materials and van der Waals heterostructures, *Science* **353**, aac9439 (2016).
- [16] Y. Liu, N. O. Weiss, X. Duan, H.-C. Cheng, Y. Huang, and X. Duan, Van der Waals heterostructures and devices, *Nat. Rev. Mater.* **1**, 16042 (2016).
- [17] P. Rivera, J. R. Schaibley, A. M. Jones, J. S. Ross, S. Wu, G. Aivazian, P. Klement, K. Seyler, G. Clark, N. J. Ghimire, J. Yan, D. G. Mandrus, W. Yao, and X. Xu, Observation of long-lived interlayer excitons in monolayer MoSe₂-WSe₂ heterostructures, *Nat. Commun.* **6**, 6242 (2015).
- [18] D. Pierucci, H. Henck, J. Avila, A. Balan, C. H. Naylor, G. Patriarcho, Y. J. Dappe, M. G. Silly, F. Sirotti, A. T. C. Johnson, M. C. Asensio, and A. Ouerghi, Band alignment and minigaps in monolayer MoS₂-graphene van der Waals heterostructures, *Nano Lett.* **16**, 4054 (2016).
- [19] K. S. Novoselov, E. McCann, S. V. Morozov, V. I. Fal'ko, M. I. Katsnelson, U. Zeitler, D. Jiang, F. Schedin, and A. K. Geim, Unconventional quantum Hall effect and Berry's phase of 2π in bilayer graphene, *Nat. Phys.* **2**, 177 (2006).
- [20] Y. A. Bychkov and E. I. Rashba, Properties of a 2D electron gas with lifted spectral degeneracy, *JETP Lett.* **39**, 78 (1984).
- [21] J. Nitta, T. Akazaki, H. Takayanagi, and T. Enoki, Gate Control of Spin-Orbit Interaction in an Inverted In_{0.53}Ga_{0.47}As/In_{0.52}Al_{0.48}As Heterostructure, *Phys. Rev. Lett.* **78**, 1335 (1997).
- [22] I. Žutić, J. Fabian, and S. Das Sarma, Spintronics: Fundamentals and applications, *Rev. Mod. Phys.* **76**, 323 (2004).
- [23] S. LaShell, B. A. McDougall, and E. Jensen, Spin Splitting of an Au(111) Surface State Band Observed with Angle Resolved Photoelectron Spectroscopy, *Phys. Rev. Lett.* **77**, 3419 (1996).
- [24] Y. M. Koroteev, G. Bihlmayer, J. E. Gayone, E. V. Chulkov, S. Blügel, P. M. Echenique, and P. Hofmann, Strong Spin-Orbit Splitting on Bi Surfaces, *Phys. Rev. Lett.* **93**, 046403 (2004).
- [25] C. R. Ast, J. Henk, A. Ernst, L. Moreschini, M. C. Falub, D. Pacilé, P. Bruno, K. Kern, and M. Grioni, Giant Spin Splitting through Surface Alloying, *Phys. Rev. Lett.* **98**, 186807 (2007).
- [26] A. Kimura, E. E. Krasovskii, R. Nishimura, K. Miyamoto, T. Kadono, K. Kanomaru, E. V. Chulkov, G. Bihlmayer, K. Shimada, H. Namatame, and M. Taniguchi, Strong Rashba-Type Spin Polarization of the Photocurrent from Bulk Continuum States: Experiment and Theory for Bi(111), *Phys. Rev. Lett.* **105**, 076804 (2010).
- [27] K. Ishizaka, M. S. Bahramy, H. Murakawa, M. Sakano, T. Shimojima, T. Sonobe, K. Koizumi, S. Shin, H. Miyahara, A. Kimura, K. Miyamoto, T. Okuda, H. Namatame, M. Taniguchi, R. Arita, N. Nagaosa, K. Kobayashi, Y. Murakami, R. Kumai, Y. Kaneko, Y. Onose, and Y. Tokura, Giant Rashba-type spin splitting in bulk BiTeI, *Nat. Mater.* **10**, 521 (2011).
- [28] H. Min, J. E. Hill, N. A. Sinitsyn, B. R. Sahu, L. Kleinman, and A. H. MacDonald, Intrinsic and Rashba spin-orbit interactions in graphene sheets, *Phys. Rev. B* **74**, 165310 (2006).
- [29] S. Konschuh, M. Gmitra, and J. Fabian, Tight-binding theory of the spin-orbit coupling in graphene, *Phys. Rev. B* **82**, 245412 (2010).
- [30] Q. Liu, Y. Guo, and A. J. Freeman, Tunable Rashba effect in two-dimensional LaOBiS₂ films: Ultrathin candidates for spin field effect transistors, *Nano Lett.* **13**, 5264 (2013).
- [31] Y. C. Cheng, Z. Y. Zhu, M. Tahir, and U. Schwingenschlöggl, Spin-orbit-induced spin splittings in polar transition metal dichalcogenide monolayers, *Europhys. Lett.* **102**, 57001 (2013).
- [32] K. Lee, W. S. Yun, and J. D. Lee, Giant Rashba-type splitting in molybdenum-driven bands of MoS₂/Bi(111) heterostructure, *Phys. Rev. B* **91**, 125420 (2015).
- [33] V. Zólyomi, N. D. Drummond, and V. I. Fal'ko, Band structure and optical transitions in atomic layers of hexagonal gallium chalcogenides, *Phys. Rev. B* **87**, 195403 (2013).
- [34] X. Li, M.-W. Lin, J. Lin, B. Huang, A. A. Puzosky, C. Ma, K. Wang, W. Zhou, S. T. Pantelides, M. Chi, I. Kravchenko, J. Fowlkes, C. M. Rouleau, D. B. Geohegan, and K. Xiao, Two-dimensional GaSe/MoSe₂ misfit bilayer heterojunctions by van der Waals epitaxy, *Sci. Adv.* **2**, e1501882 (2016).
- [35] G. Kresse and D. Joubert, From ultrasoft pseudopotentials to the projector augmented-wave method, *Phys. Rev. B* **59**, 1758 (1999).
- [36] J. P. Perdew, K. Burke, and M. Ernzerhof, Generalized Gradient Approximation Made Simple, *Phys. Rev. Lett.* **77**, 3865 (1996).
- [37] S. Grimme, J. Antony, S. Ehrlich, and S. Krieg, A consistent and accurate *ab initio* parametrization of density functional dispersion correction (DFT-D) for the 94 elements H-Pu, *J. Chem. Phys.* **132**, 154104 (2010).

- [38] J. Klimes, D. R. Bowler, and A. Michaelides, Chemical accuracy for the van der Waals density functional, *J. Phys.: Condens. Matter* **22**, 022201 (2010).
- [39] J. Klimes, D. R. Bowler, and A. Michaelides, Van der Waals density functionals applied to solids, *Phys. Rev. B* **83**, 195131 (2011).
- [40] H.-P. Komsa and A. V. Krasheninnikov, Electronic structures and optical properties of realistic transition metal dichalcogenide heterostructures from first principles, *Phys. Rev. B* **88**, 085318 (2013).
- [41] P. Johari and V. B. Shenoy, Tuning the electronic properties of semiconducting transition metal dichalcogenides by applying mechanical strains, *ACS Nano* **6**, 5449 (2012).
- [42] K. He, C. Poole, K. F. Mak, and J. Shan, Experimental demonstration of continuous electronic structure tuning via strain in atomically thin MoS₂, *Nano Lett.* **13**, 2931 (2013).
- [43] H. J. Conley, B. Wang, J. I. Ziegler, R. F. Haglund, Jr., S. T. Pantelides, and K. I. Bolotin, Bandgap engineering of strained monolayer and bilayer MoS₂, *Nano Lett.* **13**, 3626 (2013).
- [44] Q. Y. Zhang, Y. C. Cheng, L.-Y. Gan, and U. Schwingenschlögl, Giant valley drifts in uniaxially strained monolayer MoS₂, *Phys. Rev. B* **88**, 245447 (2013).
- [45] J. Kang, S. Tongay, J. Zhou, J. Li, and J. Wu, Band offsets and heterostructures of two-dimensional semiconductors, *Appl. Phys. Lett.* **102**, 012111 (2013).
- [46] A. Ramasubramaniam, Large excitonic effects in monolayers of molybdenum and tungsten dichalcogenides, *Phys. Rev. B* **86**, 115409 (2012).
- [47] Y. Ma, Y. Dai, M. Guo, L. Yu, and B. Huang, Tunable electronic and dielectric behavior of GaS and GaSe monolayers, *Phys. Chem. Chem. Phys.* **15**, 7098 (2013).
- [48] A. A. Mostofi, J. R. Yates, Y.-S. Lee, I. Souza, D. Vanderbilt, and N. Marzari, Wannier90: A tool for obtaining maximally-localised Wannier functions, *Comput. Phys. Commun.* **178**, 685 (2008).
- [49] W. X. Feng, Y. G. Yao, W. G. Zhu, J. J. Zhou, W. Yao, and D. Xiao, Intrinsic spin Hall effect in monolayers of group-VI dichalcogenides: A first-principles study, *Phys. Rev. B* **86**, 165108 (2012).
- [50] C. H. Li, O. M. J. van't Erve, S. Rajput, L. Li, and B. T. Jonker, Direct comparison of current-induced spin polarization in topological insulator Bi₂Se₃ and InAs Rashba states, *Nat. Commun.* **7**, 13518 (2016).
- [51] Q. M. Shao, G. Q. Yu, Y.-W. Lan, Y. M. Shi, M.-Y. Li, C. Zheng, X. D. Zhu, L.-J. Li, P. K. Amiri, and K. L. Wang, Strong Rashba-Edelstein effect-induced spin-orbit torques in monolayer transition metal dichalcogenide/ferromagnet bilayers, *Nano Lett.* **16**, 7514 (2016).
- [52] W. Zhang, J. Sklenar, B. Hsu, W. J. Jiang, M. B. Jungfleisch, J. Xiao, F. Y. Fradin, Y. H. Liu, J. E. Pearson, J. B. Ketterson, Z. Yang, and A. Hoffmann, Research update: Spin transfer torques in permalloy on monolayer MoS₂, *APL Mater.* **4**, 032302 (2016).
- [53] Y. K. Kato, R. C. Myers, A. C. Gossard, D. D. Awschalom, Observation of the spin Hall effect in semiconductors, *Science* **306**, 1910 (2004).
- [54] J. Wunderlich, B. Kaestner, J. Sinova, and T. Jungwirth, Experimental Observation of the Spin-Hall Effect in a Two-Dimensional Spin-Orbit Coupled Semiconductor System, *Phys. Rev. Lett.* **94**, 047204 (2005).
- [55] V. Sih, R. C. Myers, Y. K. Kato, W. H. Lau, A. C. Gossard, and D. D. Awschalom, Spatial imaging of the spin Hall effect and current-induced polarization in two-dimensional electron gases, *Nat. Phys.* **1**, 31 (2005).